2. Interior stringer: This procedure requires coring 4-in.-diameter holes vertically through the lateral gusset plate on both sides of the transverse stiffener. The edge of the hole along the web plate is milled or ground to achieve the profile indicated in Figure 20. The purpose of this retrofit is to increase the gap width between the gusset plate and stiffener. This modification will reduce the stress gradient in the gap region, thereby improving the fatigue life of the detail and providing a condition that will be easier to inspect.

In conjunction with the limited retrofitting program, both routine and in-depth inspections at periodic intervals should be continued. It is recommended that routine inspections be carried out on a 2-year interval, while a 10-year interval is appropriate for the in-depth inspection.

It has been concluded that the small gap condition in the lateral gusset plate has the potential for fatigue cracking and fracture. Assuming that the recommended retrofitting is carried out and a 10-year in-depth inspection program is followed, satisfactory performance of this structure should be assured.

ACKNOWLEDGMENT

This investigative study was carried out by Wiss, Janney, Elstner Associates, Inc., for the CTA. The support provided by Thomas Wolgemuth, Pat McCarthy, and Dennis Penepacker of the CTA was especially appreciated.

REFERENCES

1. The Technical Committee. Final Report on Causes of Fractures in Bent Nos. 24, 25, and 26, Dan Ryan Rapid Transit. Department of Public Works, Chicago, 1979.
2. J.W. Fisher. Bridge Fatigue Guide--Design and Details. American Institute of Steel Construction, Chicago, 1977.
3. D.A. Platten, K.H. Frank, and J.A. Yura. Analytical Study of the Fatigue Behavior of a Longitudinal Transverse Stiffener Intersection. Res. Report 247-1. Center for Transportation Research, University of Texas, Austin, Aug. 1981.

Publication of this paper sponsored by Committee on Dynamics and Field Testing of Bridges.

Post-Construction Evaluation of the Fremont Bridge

MICHAEL J. KOOB, JOHN M. HANSON, and JOHN W. FISHER

ABSTRACT

The Fremont Bridge is a three-span, stiffened-steel tied arch that is 2,159 ft long. During construction a major brittle fracture occurred in one of the box-shaped tie girders near the end of the bridge at the beginning of the arch rib. Since completion in 1973, small cracks and other discontinuities were found in welds in the vicinity of the junction of the tie girders and arch ribs. Cracks were also found in welds that connect wide flange stiffeners to the side plates of the tie girders. A comprehensive post-construction evaluation of the bridge was made to assess the long-range integrity of main load-carrying, nonredundant tensile members and components of the structure. The study included a review of drawings and records of construction, visual inspection of the tie girders, nondestructive examination of welds, field testing, an analytical review, and examination and testing of cores. The information collected during the study, particularly the testing and examination of core samples, is reviewed. Also, the evaluation of the resistance of the bridge to fatigue and fracture is summarized. As part of this study, a surveillance plan was developed that is intended to reveal crack growth in time to take corrective action.

The Fremont Bridge is a three-span, stiffened-steel tied arch that is 2,159 ft long (Figure 1). It was designed in the late 1960s (1) to meet the requirements of the ninth edition (1965) of the AASHO Standard Specifications for Highway Bridges (2). This was before the adoption of new fatigue provisions that appeared in the 1974 AASHTO Interim Specifications (3). Construction of the bridge was completed in 1973.

Under the 1978 AASHTO fracture control plan (4), the tie girders of the Fremont Bridge are classified as main load-carrying, nonredundant tensile members. There are numerous conditions in the tie girders that can be classified as category E or E', according to current AASHTO specifications.

During construction a major brittle fracture occurred in one of the tie girders near the end of the bridge at the beginning of the arch rib. As a result of this fracture, a major modification was made in the structure at this location.

Since completion of the bridge, small cracks and other defects were found in welds in the vicinity of the junction of the tie girders and arch ribs. Cracks were also found in welds that connect wide flange stiffeners to the web plates of the girders.

A comprehensive post-construction evaluation of the Fremont Bridge was made to assess the long-range integrity of main load-carrying, nonredundant tensile members and components of the structure. The study included a review of drawings and records of construction, visual inspection of the tie girders, nondestructive examination of welds, field testing,

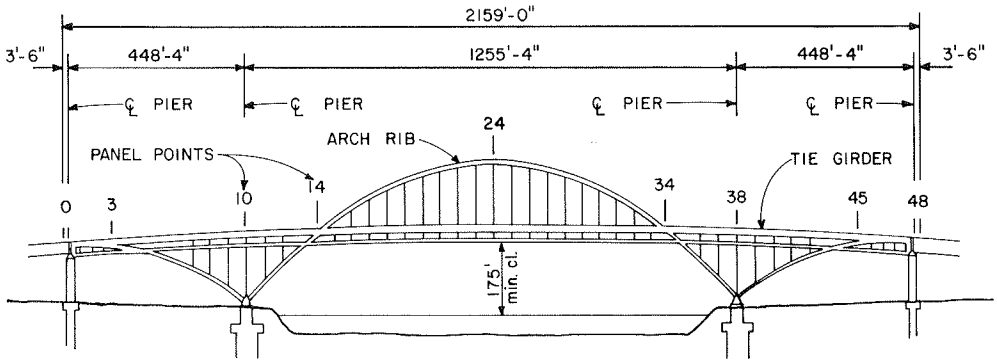

FIGURE 1 Elevation of Fremont Bridge.

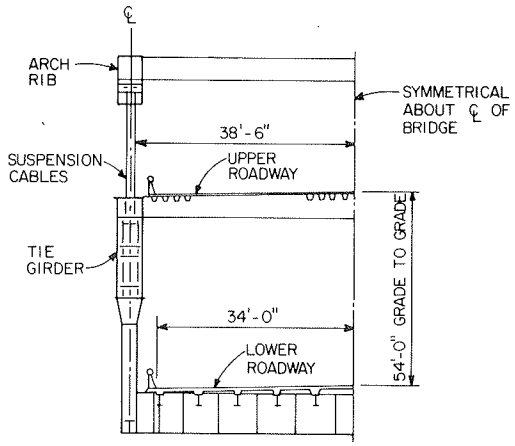

FIGURE 2 Typical section where arch is above roadway.

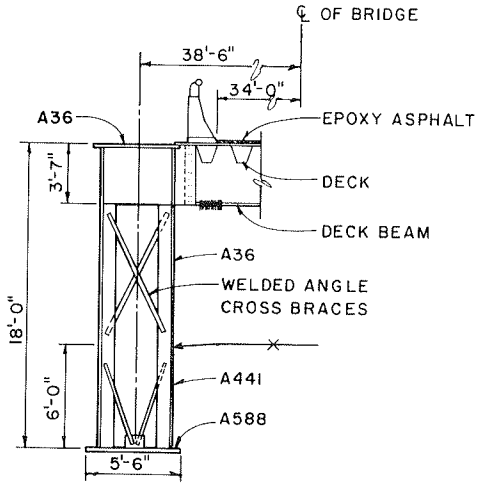

GIRDER SECTION

FIGURE 3 Representative details of tie girder.

an analytical review, and examination and testing of cores.

The information collected from the various tasks, particularly the testing and examination of core samples, is reviewed. This study was limited to the tie girders and the junction of the arch rib and tie girder. Also, the evaluation of the resistance of the bridge to fatigue and fracture is summarized. As part of this study a surveillance plan was developed that is intended to reveal crack growth in time to take corrective action.

DESCRIPTION OF BRIDGE

The main span is divided into 28 panels, and each side span is divided into 10 panels. Each panel has a length of 44 ft, 10 in. Junctions between panels are numbered 0 through 48. In this structure the arch is loaded in compression and the tie girder is loaded in tension to conteract the thrust of the arch, as well as in flexure to resist the live-load bending moments. A detailed description of the bridge and its design is given elsewhere (1).

A typical section through the bridge, in the region where the arch is above the roadway, is shown in Figure 2. The orthotropic steel upper deck, which carries four lanes of westbound traffic, acts integrally with the tie girders. The bottom deck, which carries four lanes of eastbound traffic, is a reinforced-concrete slab supported on stringers and floor beams. In the middle 896 ft of the bridge, where the arch ribs are above the tie girders, the bottom deck is suspended by hangers from the tie girders. Outside of this region the bottom deck is framed into compression struts that extend between the arch ribs and the tie girders.

Representative details of the orthotropic deck and tie girders are shown in Figure 3. The top flange is A36 steel, whereas the bottom flange is A588. The webs are 0.5 in. thick, except at the junctions with the arch ribs and pier columns. Typically, the lower 6 ft are fabricated from a high-strength, low-alloy steel that meets the requirements of ASTM A441, and the upper part is fabricated from A36 steel. This hybrid design reflects the integral action of the orthotropic deck and tie girders, with the neutral axis about 6 ft below the top flange. Welded construction is used throughout the tie girders, except for high-strength bolted field splices.

The arch ribs are box shaped and have a constant width of 4 ft, 0 in. The depth of the web plates is 3 ft, 10 in.; hence the overall depth of the arch ribs varies, depending on the flange plates, which have a maximum thickness of 2.25 in. High-strength, quenched and tempered ASTM A514 steel is used for the arch ribs, which are welded, except for bolted field splices.

At the junctions of the girders and arch ribs located at panel points 14 and 34, the cross section of the arch rib is changed from a box shape to three A514 strap plates, each 3 in. thick and 3 ft, 10 in. deep and oriented vertically. These three straps are stiffened by a welded diaphragm at mid-depth.

The straps extend through slots in the top and bottom flanges of the girder.

The center section of the bridge, from panel point 14-34, was fabricated off site, transported on barges, and erected by hydraulic jacking. A bolted splice connects the center and end sections located within the junction of the tie girder arch rib. Heavy jacking stiffeners are also welded and bolted to the sides of the tie girder in this area.

FATIGUE-SENSITIVE CONDITIONS

Several fatigue-sensitive conditions occur repeatedly in the tie girders. These conditions are shown in Figure 4a--the junction of the longitudinal and transverse stiffeners; Figure 4b--cover plates adjacent to vent openings; Figure 4c--slots in the bottom flange for lower deck hangers; and Figure 4d--the junction of deck beams and side plates. Terminations of fillet welds, which are parallel to the axis of the tie girder in Figures 4a, c, and d, are classified as category E by AASHTO specifications (5,6). Overlapping welds at the junction of longitudinal and transverse stiffeners and the heavy welds of the thick cover plates at the vent openings are particularly severe conditions.

Vent and slot openings in the bottom flange were made by flame cutting. A number of these openings contained severe notches and gouges, as shown in Figure 5. These conditions do not meet the workmanship requirements of the AASHTO Standard Specifications for Welding of Structural Steel Highway Bridges (7).

Ultrasonic testing revealed six groove welds in the A588 bottom flange of the tie girders that are not in compliance with AASHTO requirements.

FIELD TESTING

A testing program was carried out to provide information about the behavior of the bridge under traffic and environmental conditions. Strain-gauge and thermocouple instrumentation was installed at four cross sections in the vicinity of panel point 14 to obtain a measure of overall response of the bridge. Additional instrumentation was installed at locations where conditions were believed to be susceptible to fatigue crack growth. This work is described in detail in a separate paper (8).

Field testing indicated that stress ranges in the tie girders under traffic are generally less than 2 ksi, with infrequent excursions to 3 ksi. The number of cycles varies with location, but it does not exceed the average daily truck traffic. However, the temperature of plates exposed to the sun was up to 50 degrees higher than for plates in the shade, which were always close to the ambient temperature. The nominal stress varied by about 10 ksi as a result of daily thermal effects.

The bridge was also subjected to a controlled

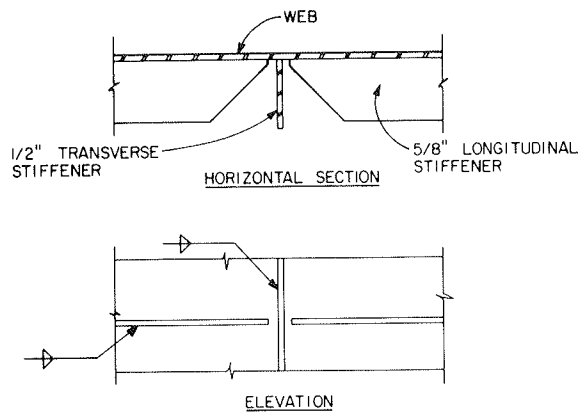

(a) Junction of longitudinal and transverse stiffeners.

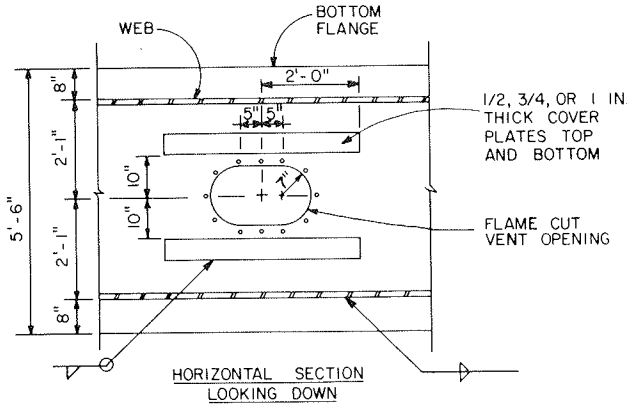

(b) Cover plates at vent opening.

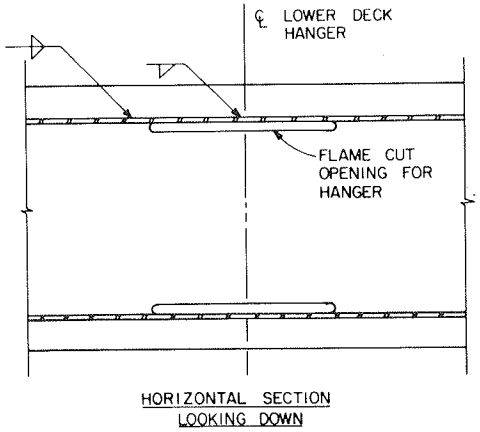

(c) Slots in bottom flange for deck hanger.

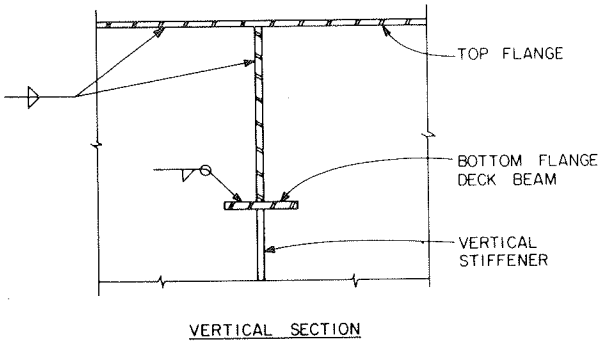

(d) Junction of deck beam and web plate.

FIGURE 4 Fatigue-sensitive conditions in tie girder.

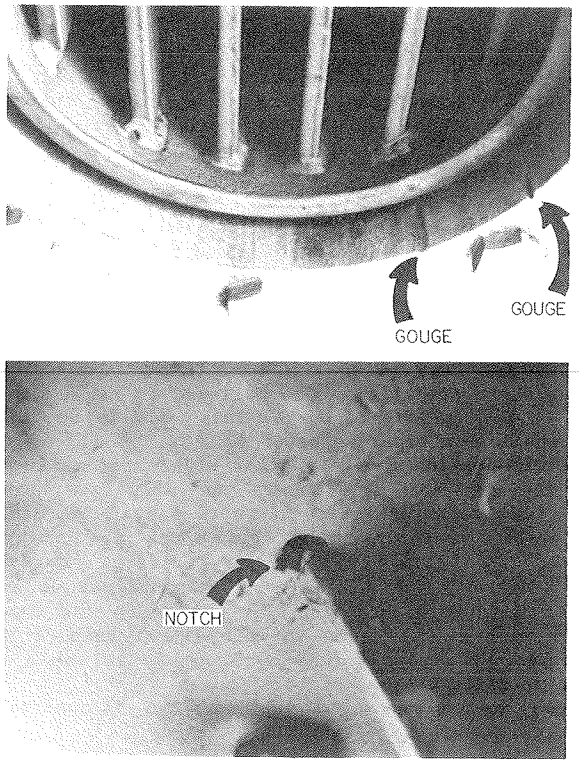

FIGURE 5 Notches and gouges on flame-cut openings: (top) vent opening in bottom flange, and (bottom) end of hanger slot.

loading test by using a group of four trucks weighing a total of 177,100 lb. Static and dynamic tests were conducted. The stress levels recorded during both tests were quite low, with the maximum recorded stress being 2.2 ksi at any instrumented location.

ANALYTICAL STUDIES

An independent design review essentially confirmed the original design and a previous review of that design. The design review was made by using a computer program developed for bridges of this type. The program considered a model of the entire bridge by using linear beam elements. Influence lines were developed for each panel point, and maximum stress ranges were computed for the live-load cases.

The maximum computed tensile stress range from an AASHTO loading on four lanes was 21.2 ksi in the bottom flange and 14.6 ksi in the top flange. For four standard HS20 trucks moving as a group across the bridge, the computed tensile stress range in the bottom flange varied from 4.0 to 5.0 ksi, and for the top flange the variation was from 0.7 to 2.9 ksi. The measured stress range was smaller because the design load condition is not representative of the actual service loads. This is recognized in the fatigue provisions of the AASHTO specifications and is the reason why only 100,000 design cycles are considered.

Following the design reveiw, a state-of-the-art finite-element analysis of the overall region from panel point 13.5 to 14.5 (the junction of the arch rib and tie girder) was carried out. The analysis did not reveal unusual force concentrations in this region.

REVIEW OF INFORMATION FROM MILL REPORTS

A diagram that shows the location of various thicknesses and types of steel plates in the tie girders is presented in Figure 6. From review of the available mill reports and the shop drawings, information was compiled relating to the heat number and the physical and chemical properties of about 90 percent of the steel plates. The mill reports for the ASTM A588 plates in the bottom flange included values of material toughness obtained from Charpy V-notch (CVN) specimens tested at +40°F in accordance with ASTM E23.

The physical and chemical properties met the requirements of the ASTM and AASHTO specifications for A36 (M183), A441 (M188), and A588 (M222) structural steels.

CVN values were obtained from the mill reports for 80 out of a total of 90 A588 bottom flange

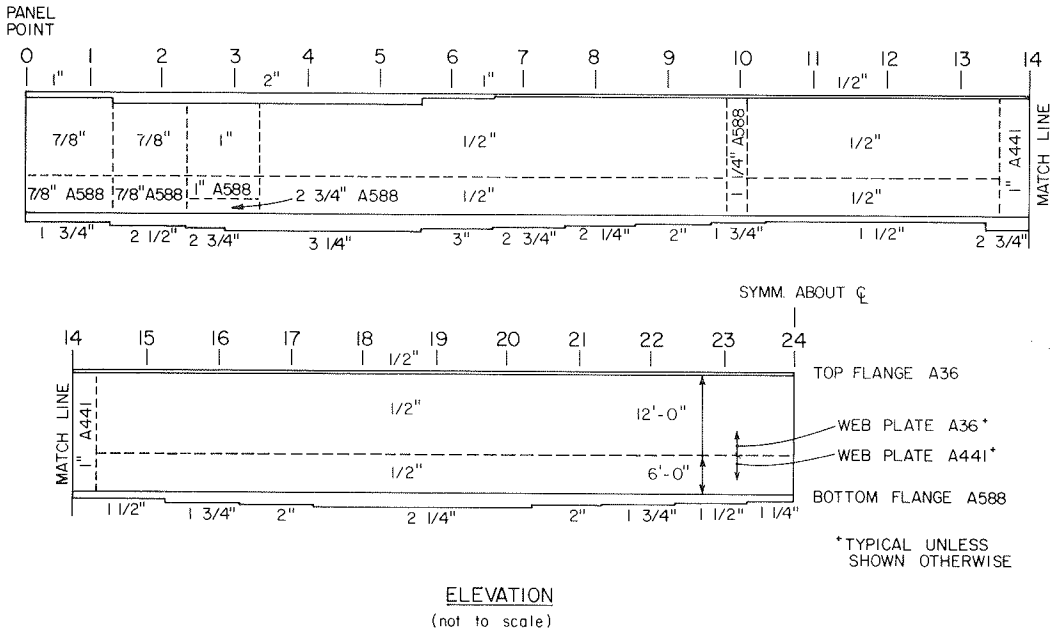

FIGURE 6 Diagram showing location and thickness of plates in tie girder.

plates. There was substantial variation in the toughness values. At three locations the values did not meet the AASHTO Guide Specifications for Fracture Critical Non-Redundant Members (4) requirements of 25 ft-lb, or 30 ft-lb for welded material more than 2 to 4 in. thick, at 40°F for zone 2. Minimum service temperature for zone 2 is from -30° to -1°F. The A588 steel at these locations came from 1.25- and 3-in.-thick material. According to the mill reports, the CVN values of the two 3-in.-thick plates were 18, 16, and 17 ft-lb at 40°F. CVN values for the 1.25-in. plate were 15, 16, and 15 ft-lb.

TESTING OF STEEL SAMPLES

Fifty cores were extracted from the tie girders of the bridge. Thirty-four 4-in.-diameter cores, along with additional plate material recovered from the location of the previous fracture near panel point 3, were used for tests to determine toughness properties. Sixteen 2- or 3-in.-diameter cores were taken from areas suspected of containing cracks or defects for metallographic and fractographic examination. This testing is described more fully in the following section.

The 4-in.-diameter core size was selected because it was adequate, after preparation, for either a special compact tension (CT) test or for machining CVN specimens. In a 0.5-in. plate, two cores were rquired at each sample location to obtain sufficient material for 12 CVN tests. Otherwise, one core sample was sufficient. Two cores were extracted at each desired sample location for a CT test in order to have replication. In general, the samples represented either common material or material that was found to have low toughness properties on the mill reports. In total, the testing program included 168 CVN tests and 20 CT tests. All of the toughness tests were conducted such that the fracture surface of the specimen was perpendicular to the longitudinal axis of the tie girder.

Two CVN specimens from each sample location were tested at each of the following temperatures: -20°, -10°, 0°, 10°, 40°, and 70°F. The results of these tests are given in Table 1. The CVN test results of

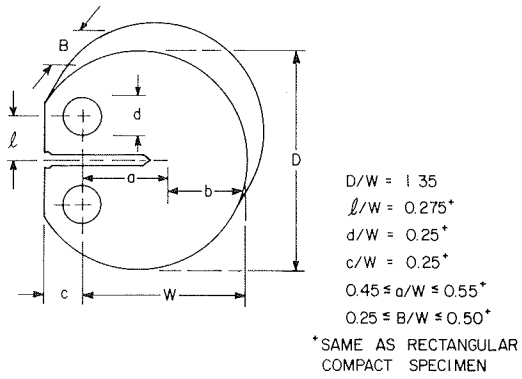

FIGURE 7 Geometry of round compact specimen.

11 and 15 ft-lb at 40°F for sample M19A taken from the 3-in.-thick A588 material confirmed the mill report values.

The 2-in.-thick A36 steel represented by sample M7A was found to have low CVN values of 7 and 8 ft-lb at 40°F. This sample represents four 2-in.-thick plates in the tie girders. It was selected for testing because the yield strength given on the mill reports was unusually high--46,900 psi.

All compact tension tests were run at -10°F, which represented the minimum service temperature for the bridge. The tests were conducted by using a time of 1 sec from zero load to failure, which represented an intermediate strain rate. Compact tension specimens made from the cores were round, as shown in Figure 7. Standard rectangular compact tension specimens were machined from the pieces of an A588 plate taken from the material recovered from panel point 3 of the previous failure, following the requirements of ASTM E399. The results of the compact tension tests are given in Table 2.

EXAMINATION OF DEFECTS

As previously indicated, sixteen 2- or 3-in.-diame-

TABLE 1 CVN Test Results

Steel Designation	Sample No.	Thickness (in.)	CVN Test Results (ft-lb) at Test Temperature (°F)					
			-20°	-10°	0°	10°	40°	70°
A36	M1A and M1B	0.5	5	8	14	21	46	99
			5	10	7	24	46	99
	M2A and M2B	0.5	5	15	26	26	58	54
			5	21	12	47	58	60
	M3A and M3B	0.5	8	8	10	10	48	69
			4	10	15	19	58	83
	M5B	1	5	8	42	54	36	82
			4	7	11	48	82	86
	M7A	2	2	3	3	4	8	13
			3	3	3	7	7	13
A441	M9A and M9B	0.5	21	13	32	44	67	84
			15	17	16	21	27	43
	M11A and M11B	0.5	6	7	21	11	39	71
			9	9	11	26	29	61
	M13A and M13B	1	5	12	13	14	31	48
			6	9	13	19	33	57
A588	M15A	1.25	8	17	16	47	66	76
			15	10	34	17	65	66
	M16A	1.5	8	10	29	23	28	84
			22	13	11	32	57	54
	M17A	1.75	13	4	8	10	37	37
			2	4	11	10	38	10
	M19A	3	11	9	6	11	11	12
			9	15	6	5	15	13
	M20A	2.5	8	6	12	50	85	
			17	26	32	45	61	
	M21A	3.25	11	4	6	19	51	72
			20	20	5	10	28	50

TABLE 2 CT Test Results

Steel Designation	Sample No.	Thickness (in.)	B (in.)	W (in.)	K_Q (ksi$\sqrt{in.}$)	ASTM E399 Validity		Stress Intensity Factor (ksi$\sqrt{in.}$)		
						P_{max}/P_Q	$2.5(K_Q/\sigma_y)^2$	K_{Ic}	K_{max}	K_J
A36	M4A	0.5	0.5	2	43.6	1.83	2.64		80.0	
	M4B	0.5	0.5	2	45.7	1.66	2.90		76.1	
	M6A	1	1	2	50.7	1.33	3.92		67.8	92.7
	M6B	1	1	2	48.8	1.59	3.62		77.6	116
	M8A	2	1.5	3	52.7	1.53	3.16		80.8	104
	M8B	2	1.5	3	55.6	1.66	3.52		92.1	130
A441	M12A	0.5	0.5	2	54.8	1.95	2.18		111	
	M12B	0.5	0.5	2	52.3	2.05	1.98		106	
	M14A	1	1	2	58.4	1.61	>1		93.9	152
	M14B	1	1	2	49.0	1.78	>1		87.3	123
A588	M18A	1.5	1.25	2.5	70.6	1.30	4.04		91.8	110
	M18B	1.5	1.25	2.5	59.2	1.08	2.84			
	M22A	3	1.5	3	57.5	1.00	1.64			
	M22B	3	1.5	3	62.2	1.00	1.92			
	M23A	2.5	2.5	5	72.6	1.25	4.10		91.1	114
	M23B	2.5	2.5	5	83.0	1.22	5.36		101	128
	M24A	3.25	3.1875	6.5		1.00	2.88	59.0[a]		
	M24B	3.25	3.1875	6.5	74.7	1.00	4.63			
	M25A	2.75	2.5	5	74.4	1.00	3.99			
	M25B	2.75	2.5	5	70.1	1.00	3.54			

Note: B = specimen thickness, W = specimen depth, K_{Ic} = critical stress intensity factor, K_Q = critical stress intensity factor (conditional result), K_{max} = critical stress intensity factor (based on P_{max}), and K_J = J integral stress intensity factor.

[a]Test result meets ASTM E399 validity requirement.

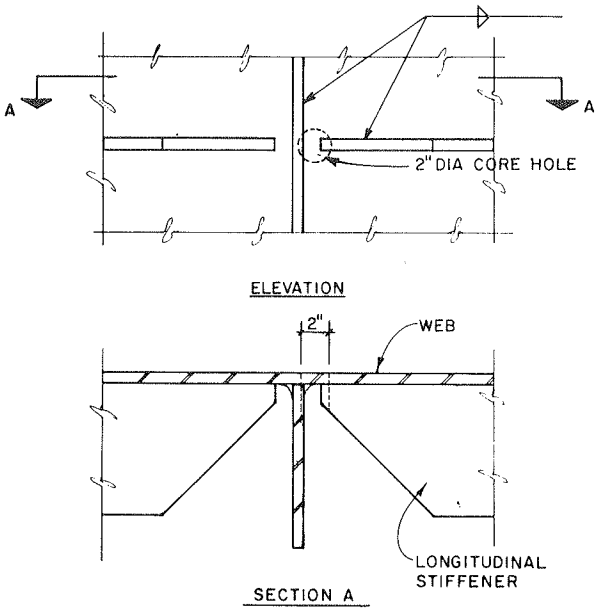

(a) C1 cores at ends of horizontal stiffeners.

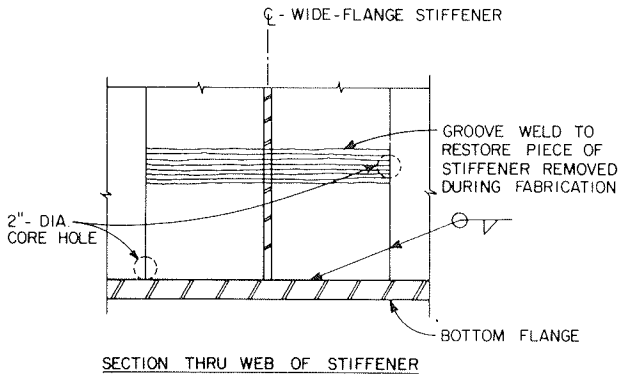

(b) C2 cores at base of wide flange stiffeners.

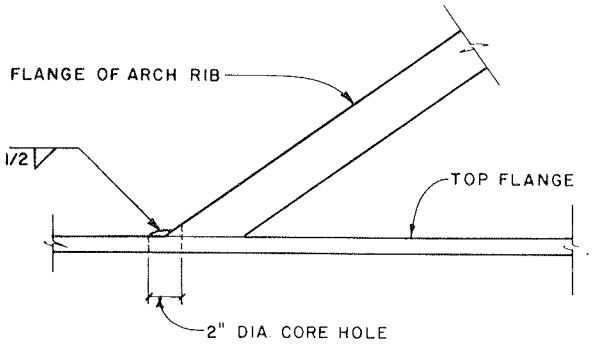

(c) C3 cores through welds at the junction of the arch rib and top and bottom flanges of the tie girder.

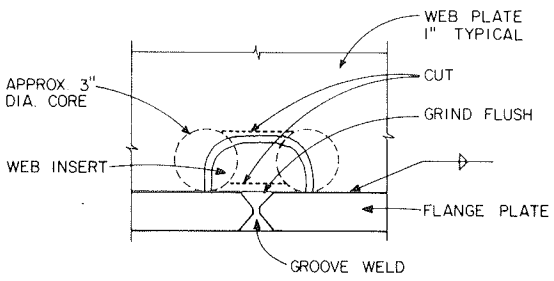

(d) C4 cores through welded inserts in web plate.

FIGURE 8 Regions where cores were extracted for examination.

ter cores were taken from locations representing four different conditions in the bridge (Figure 8) for metallographic and fractographic examinations. These samples were from locations where visual inspection had indicated a possible discontinuity.

Cores From Ends of Longitudinal Stiffeners

Four cores were removed from the junction of longitudinal and transverse stiffeners, cut into segments, and examined. The only significant defect was found at a weld overlap, where there was entrapped slag and a small crack, which may have occurred during fabrication or handling. This condition is shown in Figure 9. No evidence of fatigue crack propagation was detected when the crack was split open for examination.

Cores in Welds of Wide Flange Stiffeners

These cores were also cut into segments. Significant root cracking was present in all four cores, where the fillet welds connected the stiffener flange to the girder web. A typical root crack is visible in Figure 10. This crack originated from the sharp slag pocket at the vertical weld root.

It was evident that cracking at wide flange stiffener connections had developed at the time of fabrication. Two out of the four cores exhibited fatigue crack growth with a striation spacing of about 10^{-6} in. per cycle. This striation spacing indicated that the crack growth rate was near the lower limit detectable by fractographic examination. These cracks were not considered to be significant. Growth was the result of stress passing from the web plate into the stiffener through the vertical fillet

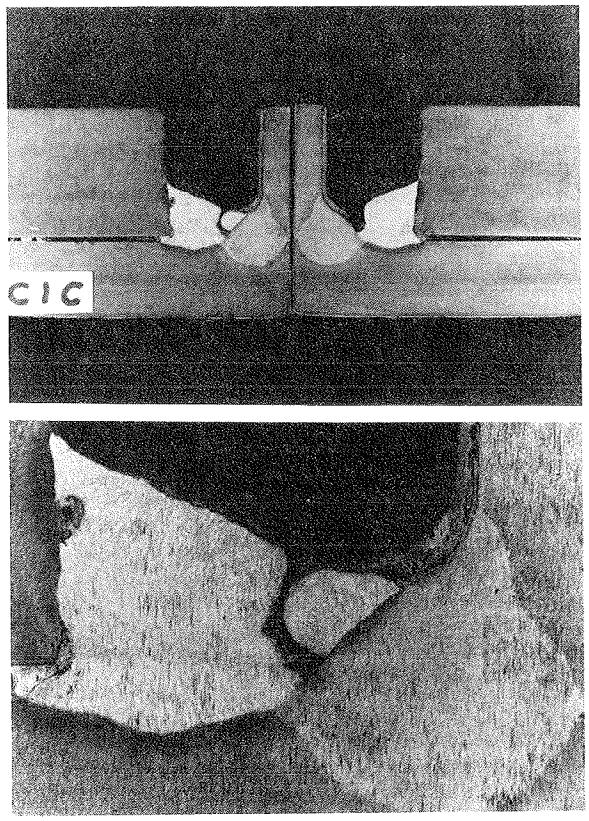

FIGURE 9 Split segments from core C1C: (top) etched cross section showing lack of fusion, and (bottom) close-up showing slag and crack in weld overlap.

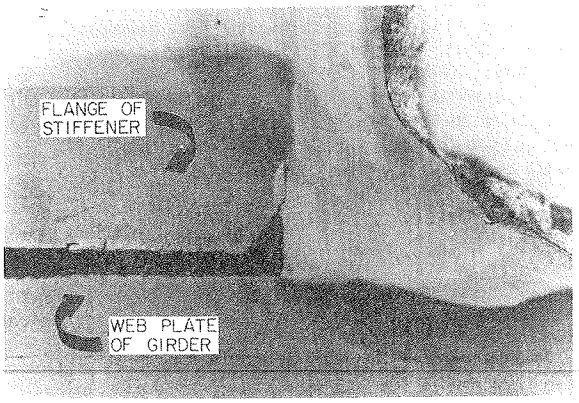

FIGURE 10 Etched surface of split segment of core C2D showing root crack from slag pocket.

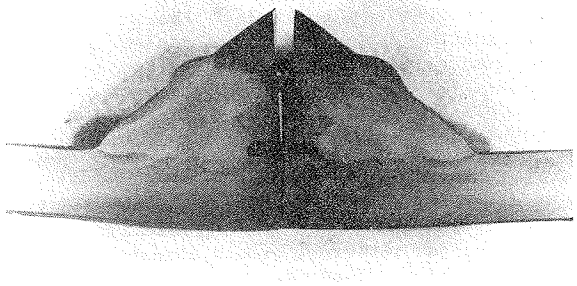

FIGURE 11 Etched sections of sample core C3C showing insert plate and notches at weld roots.

welds, promoted by the existence of extensive weld root cracking. However, the crack propagates along the leg attached to be stiffener, and the lack of fusion gap between the web and stiffener flange prevents it from moving into the girder web and creating a more serious crack condition.

Core Through Welds at Junction of Arch Rib and Flanges of Tie Girders

Four cores were extracted and cut into segments for examination. There was no evidence of cracking in any of the weldments, although it was visually apparent that sharp notch conditions exist at the weld roots. A substantial gap was present in all of the core samples between the flange and the arch rib plates. In one sample a 0.3125-in. plate was found to have been inserted to fill part of the gap between the arch rib and top flange before welding. The weld fused the insert plate and the arch rib and tie girder flanges, as shown in Figure 11. However, sharp notches were found at two locations. Slag was also apparent at the root of the weldments that connect each plate. Although no sign of cracking was detected at the weld root, the distance between the root and the outside surface was only 0.3125 in. in this core. This small ligament may be susceptible to cracking.

Cores From Welded Inserts in Webs

Two pairs of cores were removed from small insert plates welded into cope holes in the web, as illustrated in Figure 8d. These holes were made during

fabrication of the groove welds in the flange. The cores were sliced into segments for examination. It appeared that the welds were intended to be double V-grooves, but the root pass was not back-gouged. There was evidence of some fatigue crack growth from the larger defects. The striation spacing suggested that fatigue crack propagation was near the crack growth threshold.

EVALUATION OF POTENTIAL FOR FRACTURE

In recent years substantial research has been directed toward evaluation of the resistance of welded steel bridges to fatigue and fracture. This research has provided the basis for the current provisions on fatigue and fracture in the AASHTO specifications.

In principle it is possible to establish relationships between flaws or defects in a steel structure and the conditions under which brittle fracture may occur by using fracture mechanics. In practice, however, it must be recognized that there is variability in the properties of steel and difficulties in defining defects, as well as theoretical limitations, on this relatively new technology.

Virtually all welded steel bridges contain discontinuities that are built into the structure during fabrication. Such discontinuities occur from lack of fusion, porosity, toe cracks, or even a weld arc strike. In addition, the geometry of the welded connections also induces stress concentrations.

Discontinuities oriented parallel to the primary stress generally do not cause problems. However, even extremely small discontinuities may induce crack growth if they are oriented perpendicular to the stress flow and the cyclic stress range is large enough to exceed the crack growth threshold.

Under repeated loading, crack propagation may occur at low stress ranges, especially if occasional higher stress ranges also occur. The rate of crack propagation depends on ΔK, the range of stress intensity at the crack tip. The stress intensity range (ΔK) may be computed as follows (9):

$$\Delta K = F(a)\, S_r \sqrt{\pi a} \qquad (1)$$

where S_r is the nominal uniform stress range, and a is the crack length. The parameter F(a) varies, depending on crack size, orientation, and shape, as well as loading conditions.

During the field testing measured peak cyclic stresses from traffic were typically less than 1 ksi and almost always less than 2 ksi for the tie girders. For small initial defects, ΔK computed from Equation 1 is about 2.5 ksi $\sqrt{\text{in.}}$ for a stress range of 10 ksi. A value of ΔK equal to 2.5 ksi $\sqrt{\text{in.}}$ is generally considered to be close to the threshold value for fatigue crack propagation. The examination of the cores supported the position that crack extension was occurring near the threshold value.

Stress intensity factors for simple crack geometries (9) are given in Figure 12. These factors are complex for most other geometries, but solutions are available in the technical literature.

Fatigue cracks that grow from fillet welds usually have a semielliptical-shaped crack front. This condition is shown in Figure 12b, where K_I is the stress intensity factor for mode I behavior. Assuming as an example that a equal to 0.20 in. and a/2c equal to 0.25 represent a small semielliptical surface crack, and taking Q equal to 1.25, K_I is approximately 0.8 S_r, or S_r is approximately 3 ksi for for ΔK equal to 2.5 ksi $\sqrt{\text{in.}}$ Assuming larger and less tolerable defects leads to lower values of S_r. Recognizing that these stress ranges are comparable to the maximum values measured under traffic in the bridge, it is not likely that crack growth will occur from the observed defect conditions that existed in the girders. The only observed crack propagation was at larger cracks, such as shown in Figure 10.

The propagation rate for cracks in ferrite-pearlite steels (10), which includes the A36, A441, and A588 steels in the tie girders, may be computed from

$$da/dN = 3.6 \times 10^{-10} (\Delta K_I)^3 \qquad (2)$$

where ΔK_I is the stress intensity factor range in ksi $\sqrt{\text{in.}}$, and da/dN is the crack growth per cycle. At a small defect and at threshold level conditions, with $\Delta K_I = 2.5$, crack growth would be expected to occur at 56×10^{-10} in. per cycle. Therefore, in 2 million cycles, for example, the crack extension would be

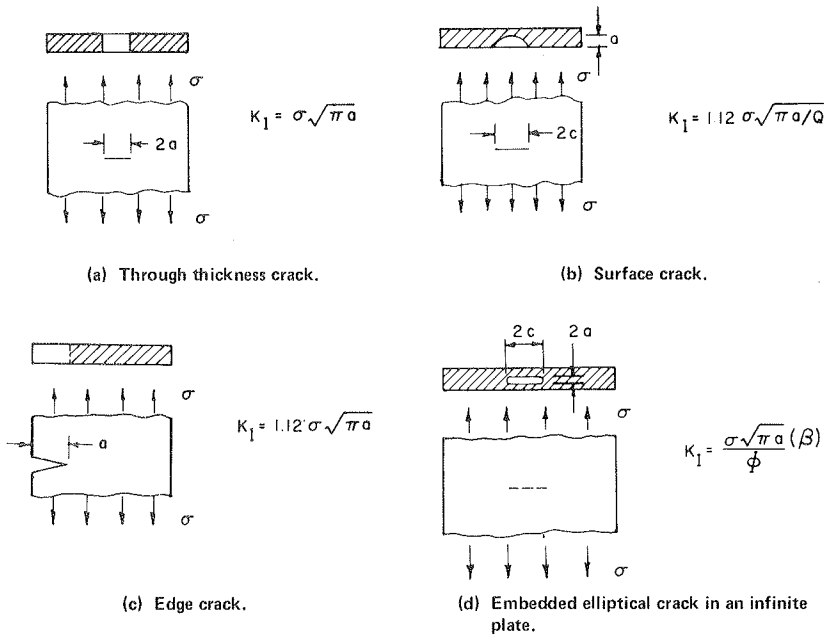

(a) Through thickness crack.

(b) Surface crack.

(c) Edge crack.

(d) Embedded elliptical crack in an infinite plate.

FIGURE 12 Simple intensity factor for simple crack geometries.

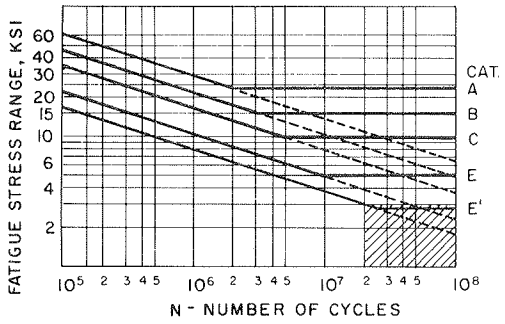

FIGURE 13 Fatigue strength of welded details.

small--about 0.02 in. Larger initial defects would have increased propagation rates.

Although the stress ranges from traffic on the Fremont Bridge are apparently close to and possibly below the threshold levels if the defects are small, a relatively high daily stress cycle caused by temperature is imposed on the traffic stress cycles. According to recent data, these large-magnitude, low-cycle stress ranges may result in crack growth in the low-magnitude, high-cycle stress ranges (11).

Test data on the fatigue strength of various details are presented in Figure 13, where the lines for the various categories are 95 percent confidence limits for 95 percent survival (12). The solid horizontal lines are considered to be a threshold uniform stress range (S_{rth}) for these categories. That is, for stress ranges below S_{rth}, crack growth does not occur and no damage to the structural detail is expected. However, for variable magnitude stress cycles, it is recommended that the dashed extension of the line be used to evaluate fatigue strength when ocassional stress cycles in the variable spectrum exceed S_{rth} (11).

Assuming that the effective stress range is 2 ksi or less, including the daily thermal effect, and that the conditions in the girders are not or can be upgraded to not worse than category E', it appears that 60 million or more cycles would be required to reach the lower bound of fatigue life. This region is cross-hatched in Figure 13.

As a result of the field testing a rough estimate of an effective Miners high-cycle stress range was developed that was expected to occur approximately 3,000 times per day. It was noted that this cycle rate was equal to about 55 percent of the average daily truck traffic. On this basis the Frement Bridge is currently being subjected to approximately 1 million cycles of low-magnitude, high-cycle stress range per year that may be capable of producing crack growth in details with relatively small defects.

As a crack propagates, the stress intensity factor increases until it reaches a critical value (K_{Ic}). At this value the propagation becomes unstable and brittle fracture occurs. The physical testing program that was described previously was intended to provide test results to establish K_{Ic}. However, only one test result reported in Table 2, from sample M24A, met the validity requirements of ASTM E399 for considering K_Q to be equal to K_{Ic}. This sample was obtained from A588 steel recovered from the bottom flange of the girder that sustained the fracture during construction.

The values of K_Q for all of the samples from the A36 and A441 steels were invalid estimates of K_{Ic} because the ratio P_{max}/P_Q was greater than 1.10. This indicates that the steel was tougher than the estimate provided by K_Q.

For the A588 steel, samples M18A, M23A, and M23B failed to meet the requirement that the thickness of the specimen (B) shall be greater than 2.5 $(K_Q/\sigma_y)^2$ as well as the requirement that P_{max}/P_Q shall be less than 1.10. All of the other invalid results on A588 steel failed to meet the requirement for maximum thickness. However, it should be noted that all of the samples failing to meet the requirement, except for M22A and M22B, were tested in full plate thickness; therefore, K_Q should be a satisfactory estimate for K_{Ic}. Further, the thickness of samples M22A and M22B was close to the ratio of 2.5 $(K_Q/\sigma_y)^2$, and the results are probably valid.

Based on review of the test results, K_{Ic} was assumed equal to 80 ksi $\sqrt{in.}$ for the A36 and A441 steels and 60 ksi $\sqrt{in.}$ for the A588 steel in the evaluation of fracture resistance of the tie girders.

Critical crack dimensions for the simple crack geometrics shown in Figure 12 were computed based on K_I equal to 60 or 80 ksi $\sqrt{in.}$ For a crack or defect near a weld, it was assumed that the in situ stress was equal to the yield stress because of the residual shrinkage stress associated with the weld. For defects away from welds, the in situ stress was considered equal to the dead-load stress plus an allowance for thermal effects on the tie girders. Assuming that this allowance for thermal effects is approximately 10 ksi (as measured during the field testing program), the maximum nominal stress for defects not associated with welds was taken to be equal to 0.55 σ_y for all three steels. Critical crack dimensions based on these assumptions are given in Table 3.

TABLE 3 Critical Crack Dimensions

Crack or Defect Geometry	Type of Steel	Critical Crack Dimension[a] (in.) Near Welds[b]	Away From Welds[c]
Through thickness crack (2a)	A36	3.25	10
	A441	1.75	5.25
	A588	1	3
Surface crack with a/2c = 0.1 (a)	A36	1.1	3.6
	A441	0.6	2.0
	A588	0.3	1.1
Edge crack (a)	A36	1.25	4.0
	A441	0.75	2.25
	A588	0.50	1.25
Embedded elliptical crack, a/c = 0.25 (2a)	A36	3.75	11.75
	A441	2.0	6.25
	A558	1.0	3.5

[a] Assuming K_{Ic} = 80 ksi$\sqrt{in.}$ for A36 and A441 steel and K_{Ic} = 60 ksi$\sqrt{in.}$ for A588 steel.
[b] Assuming $\sigma = \sigma_y$.
[c] Assuming $\sigma = 0.55\ \sigma_y$.

CONCLUDING REMARKS

The Fremont Bridge contains low-toughness steel that does not meet current AASHTO specifications. Also, the computed stress ranges under the prescribed loadings of the specifications exceed the allowable design stress range limits. However, the measured stress ranges from traffic are smaller than stress ranges that correspond to the fatigue limit for the worst details. Only the thermal stress cycle was observed to exceed the crack growth threshold. Therefore, the principal conclusion of the evaluation is that a long period of time, on the order of 60 years, is required before there should be any potential for significant fatigue crack propagation within the tie girders, provided there are no existing defects of greater size and sharpness than normally are associated with category E or E' conditions.

Recommendations were made to reduce the severity

of all potentially critical fatigue and fracture conditions, including grinding severe gouges in all of the flame-cut openings and shot-peening weld terminations. The weld around the junction of the arch rib and exterior flange surfaces was to be removed by grinding or milling. The exterior arch rib straps are to be bolted to the webs of the girder to offset the removal of the weld around the junction. An in-depth visual inspection with nondestructive testing was recommended along with work to reduce the severity of the critical conditions.

Future in-depth inspections were also recommended beyond those normally performed in maintaining a bridge. These inspections should be performed at intervals of about 10 years. Because paint would be removed and light grinding would be carried out at critical locations during this work, it appears to be advisable to coordinate these in-depth inspections with repainting of the tie girders.

ACKNOWLEDGMENT

This post-construction evaluation of the Fremont Bridge was carried out by Wiss, Janney, Elstner Associates, Inc. (WJE) for the Oregon State Highway Division. The study was supported by the FHWA. WJE was assisted by John W. Fisher; Ammann and Whitney; Testing Engineers, Inc.; and Materials Research Laboratory, Inc. A technical committee met periodically during the study under the chairmanship of Walter J. Hart, bridge engineer for the state of Oregon.

REFERENCES

1. A. Hedefine and L.G. Silano. Design of the Fremont Bridge. Preprint 1210. Presented at the ASCE National Structural Engineering Meeting, Portland, Oreg., April 1970.
2. Standard Specifications for Highway Bridges, 9th ed. AASHO, Washington, D.C., 1965.
3. Interim Specifications, Bridges. AASHTO, Washington, D.C., 1974.
4. Guide Specifications for Fracture Critical Non-Redundant Steel Bridge Members. AASHTO, Washington, D.C., Sept. 1978.
5. Standard Specifications for Highway Bridges, 12th ed. AASHTO, Washington, D.C., 1977.
6. Interim Specifications for Highway Bridges. AASHTO, Washington, D.C., 1979.
7. Standard Specifications for Welding of Structural Steel Highway Bridges, 2nd ed. AASHTO, Washington, D.C., 1977.
8. M.J. Koob and J.M. Hanson. Field Testing of the Fremont Bridge. In Transportation Research Record 903, TRB, National Research Council, Washington, D.C., 1983, pp. 1-8.
9. R. Roberts, J.M. Barsom, J.W. Fisher, and S.T. Rolfe. Fracture Mechanics for Bridge Design. FHWA, U.S. Department of Transportation, July 1977.
10. S.T. Rolfe and J.M. Barsom. Fatigue and Fracture Control in Structures: Applications of Fracture Mechanics. Prentice-Hall, Englewood Cliffs, N.J., 1977.
11. J.W. Fisher, D.R. Mertz, and A. Zhong. Steel Bridge Members Under Variable Amplitude, Long Life Fatigue Loading. NCHRP Report 267. TRB, National Research Council, Washington, D.C., Dec. 1983, 26 pp.
12. J.W. Fisher. Bridge Fatigue Guide--Design and Details. American Institute of Steel Construction, Chicago, 1977.

Publication of this paper sponsored by Committee on Dynamics and Field Testing of Bridges.